

## A Structure–Property Relationship Study of the Well-Defined Telodendrimers to Improve Hemocompatibility of Nanocarriers for Anticancer Drug Delivery

Changying Shi,<sup>†,⊥</sup> Dekai Yuan,<sup>‡,||,⊥</sup> Shikha Nangia,<sup>§</sup> Gaofei Xu,<sup>†,‡</sup> Kit S. Lam,<sup>||</sup> and Juntao Luo<sup>†,\*</sup>

<sup>†</sup>Department of Pharmacology, SUNY Upstate Cancer Research Institute, State University of New York Upstate Medical University, 750 East Adams Street, Syracuse, New York 13210, United States

<sup>‡</sup>Department of Applied Chemistry, College of Science, China Agricultural University, Beijing, 100193, China

<sup>§</sup>Department of Biomedical and Chemical Engineering and Syracuse Biomaterials Institute, Syracuse University, Syracuse, New York 13244, United States

<sup>||</sup>Department of Biochemistry and Molecular Medicine, School of Medicine, University of California, Davis, Sacramento, California 95817, United States

### Supporting Information

**ABSTRACT:** A series of telodendrimer (a linear polyethylene glycol-*b*-dendritic oligo-cholic acid) have been synthesized via a bottom-up approach to optimize the hemocompatibility of the nanocarrier. Numbers of hydrophilic glycerol groups were introduced onto the polar surface of cholic acid to reduce the plasma membrane lytic activity of telodendrimers. An interesting result was observed: only an optimum number of glycerol introduced could reduce the hemolytic properties of the nanocarrier; on the contrary, more glycerols or the amino-glycerol substitution onto cholic acid significantly increased the hemolytic properties of the nanocarriers.

To further elucidate the structure–property relationship, the molecular dynamic approach was used to simulate the conformation of the subunits of telodendrimers with different glycerol substitution, and the binding energies and the polar surface areas of the hairpin conformations were calculated to explain the membrane activities of nanocarriers. In addition, these telodendrimer subunits were synthesized and their membrane activities were tested directly, which validated the computational prediction and correlated with the observed hemolytic activity of nanocarriers. The glycerol substitution sustained the facial amphiphilicity of cholic acid, maintaining the superior drug loading capacity (paclitaxel and doxorubicin), stability, cell uptake, and anticancer efficacy of payloads. The *in vivo* optical imaging study indicated that the optimized nanocarriers can specifically deliver drug molecules to the tumor sites more efficiently than free drug administration, which is essential for the enhanced cancer treatment.



## INTRODUCTION

The structure and property relationship (SPR) in polymer nanocarriers are normally hard to be defined clearly, due to the polydispersity of polymer and the limited capability for the site-specific functionalization. In contrast, the biomacromolecule systems, e.g. peptide, protein, and the oligonucleotides have a precise structure (sequence)–property relationship in regulating the activities of the biologics. It is clear that the well-defined structures of materials are essential for the quantitative analysis of the SPR in functional materials and allow for the application of the theoretical and computational approaches to rationally design and predict the properties of the nanocarriers. These approaches would significantly accelerate the development of the efficient nanocarriers for drug delivery, compared with the empirical approaches in nanocarrier development. This is in line with the effort of the “material genome initiative” launched by the White House of the U.S. government in 2011.

Anticancer drugs encapsulated in nanoparticles, e.g. liposomes, polymer micelles, and polymer nanoparticles, are

normally administered via intravenous injections that require the nanocarriers to be hemocompatible and have stealth property in order to avoid fast clearance by the reticuloendothelial system (RES). The formation of the nanocarriers is mostly driven by the hydrophobic aggregation or ionic interactions of the amphiphilic materials, which have a tendency to interact with cell membranes via hydrophobic or charge interactions.<sup>1–3</sup> Such plasma membrane lytic activity may raise safety issues for *in vivo* applications of nanocarriers. Synthetic amphiphilic polymers have been synthesized to form micelle nanocarriers for drug delivery.<sup>4</sup> To elucidate the SPR in membrane activity is crucial in optimizing the nanocarrier for safe and efficient *in vivo* drug delivery. We have developed a biohybrid system, i.e. poly(ethylene glycol)-*b*-dendritic oligocholic acid (CA) (named as telodendrimer) via peptide

Received: January 27, 2014

Revised: March 5, 2014

Published: May 21, 2014

chemistry.<sup>5</sup> It has a well-defined structure with the capability of the precise structural design and functionalization. Telodendrimers self-assemble into stable micelles for efficient paclitaxel (PTX) encapsulation<sup>6</sup> and a few other anticancer drugs (see citations in Supporting Information [SI]). While the paclitaxel-loaded micelles formed by such telodendrimers exhibited a safe profile in *in vivo* administration for anticancer treatment in mouse models and companion dogs, the empty telodendrimer micelles showed moderate hemolytic properties at relative high concentrations (1 mg/mL) *in vitro*. The former can be explained by enhanced hydrophobic interactions within the nanotherapeutics by loading highly hydrophobic PTX. However, the loading of some other drug molecules may not be able to stabilize the micelle and may result in hemolysis when given intravenously. The cross-linking approaches are able to stabilize micelles and reduce hemolytic properties.<sup>7,8</sup> However, the additional reagents and treatments for micelle cross-linking usually require extensive purification before *in vivo* administration, which may lead to the loss of drug molecules and will be a significant burden for clinical application in terms of quality control and regulations. Therefore, there is a need to study the structure and hemolytic activity relationship of nanocarrier to eliminate the hemolytic potential, which could be studied via a series of structural modifications and the property characterization.

Cholic acid, the key building block in telodendrimers, is known to have strong membrane activity as a small-molecule surfactant.<sup>9</sup> The stacking between the hydrophilic surfaces of cholic acid units via hydrogen bonding is essential to shelter the polar groups allowing for the insertion of a whole complex into the hydrophobic phospholipids bilayer membrane.<sup>10</sup> We hypothesize that introducing bulky hydrophilic groups onto hydroxyl groups of CA may disrupt the compact interactions between the polar surfaces of CAs and increase the polar surface area (PSA) of the whole complex, therefore reducing the membrane activity of telodendrimers. In order to modify the telodendrimer with a well-defined structure, we chose the bottom-up approach to modify cholic acid before being conjugated onto the telodendrimer. Glycerol or amino glycerol groups are introduced onto the cholic acid via ether bond formation with hydroxyl groups at the 3- and 7- or 12-positions. The core-forming subunits of the telodendrimers have been studied via molecular dynamics to study the conformations and the corresponding polar surface area (PSA) to predict the membrane activities of the nanocarriers. Further, the telodendrimer subunits with different glycerol substitution were synthesized directly and the membrane activities were tested to validate the theoretical predictions. The anticancer drugs, paclitaxel (PTX) and doxorubicin (DOX), were successfully loaded into the modified telodendrimer micelles. The drug loading capacity, stability, tumor targeting, and anticancer effects were systematically studied *in vitro* and *in vivo*.

## ■ EXPERIMENTAL SECTION

**Materials and Instruments.** Monomethylterminated poly(ethylene glycol) monoamine hydrochloride(MeO-PEG-NH<sub>2</sub>·HCl,  $M_w$ : 5000 Da) was purchased from Jenkem Technology (Dallas, TX). (Fmoc)Lys(Fmoc)-OH was obtained from AnaSpec Inc. (San Jose, CA). Paclitaxel (PTX) was purchased from AK Scientific (Union City, CA). NIRF dye DiD (1,1'-dioctadecyl-3,3,3',3'-tetramethylindodicarbocyanine perchlorate, D-307), was purchased from Invitrogen. Tetrazolium compound [3-(4,5-dimethylthiazol-2-yl)-5-(3-carboxymethoxyphenyl)-2-(4-sulfophenyl)-2H-tetrazolium, MTS] and phenazine methosulfate (PMS) were purchased from Promega (Madison, WI).

Cholic acid (CA), epichlorohydrin, diisopropyl carbodiimide (DIC), N-hydroxybenzotriazole (HOBr), and all other chemicals were purchased from Sigma-Aldrich (St. Louis, MO). Molecular dynamics simulations were carried out using the freely distributed Gromacs 4.5.5 software package.<sup>11</sup> <sup>1</sup>H NMR spectra of the small molecules and polymers were recorded using Bruker AVANCE 600 MHz spectrometer in CDCl<sub>3</sub> or DMSO-*d*<sub>6</sub>. Particle sizes of micelle were measured using a dynamic lighter scattering (DLS) particle sizer (Zetatrac, Microtrac Inc.) and the area-based mean particle sizes were presented. The TEM images of micelles were recorded on a transmission electron microscope (JEOL JEM-2100) and samples were stained with uranyl acetate. A UV-vis Nanodrop spectrometer and a Simadzu HPLC (LC20AT) equipped with a C18 column and 55% MeCN as mobile phase were used for detection of drug loading efficiency and drug release studies. Fortessa (Becton Dickinson, San Jose, CA) flow cytometer was used for cell uptake study, and IVIS-200 small animal imager was used for *in vivo* tumor imaging.

The nomenclature of the telodendrimers and the dimer molecules followed the system used in the previous studies: For example, telodendrimer PEG<sup>sk</sup>CA<sub>8</sub> indicates that the molecular weight of PEG is 5 kDa and there are eight cholic acids conjugated on the periphery of dendritic polylysine. The additional functional groups on CA were described as CA-4OH, CA-5OH, CA-3OH-NH<sub>2</sub>, representing one glycerol, two glycerols and one animoglycerol introduced onto cholic acid, respectively. The corresponding telodendrimers were named as PEG<sup>sk</sup>(CA-4OH)<sub>8</sub>, PEG<sup>sk</sup>(CA-5OH)<sub>8</sub>, PEG<sup>sk</sup>(CA-3OH-NH<sub>2</sub>)<sub>8</sub>. The dimer molecules were synthesized from CA and CA derivatives via a lysine (K in abbreviation) bridge and named as KCA<sub>2</sub>, K(CA-4OH)<sub>2</sub>, K(CA-5OH)<sub>2</sub>. The preparations of cholic acid derivatives and the dimer molecules are described in SI.

**Preparation of Telodendrimers.** As reported in our previous procedure,<sup>5</sup> telodendrimers have been prepared from MeOPEG-NH<sub>2</sub> with 5000 Da molecular weight via stepwise solution phase Fmoc-peptide chemistry. Briefly, Fmoc peptide chemistry was used to couple (Fmoc)Lys(Fmoc)-OH onto the N-terminal of PEG (MW = 5 or 10 kDa) using diisopropyl carbodiimide (DIC, 3 equiv) and N-hydroxybenzotriazole (HOBr, 3 equiv) as coupling reagents in DMF overnight. Upon confirmation of negative results from the Kaiser test for the reaction, chilled ether was added to the reaction solution to precipitate out the polymer, which was further washed twice with chilled ether. Fmoc protecting groups were removed by treatment with 20% piperidine in DMF for 30 min, and polymer was precipitated and washed with cold ether. After three steps of repeated coupling of (Fmoc)lysine(Fmoc)-OH and de-Fmoc reactions, a dendritic polylysine was synthesized at one end of PEG. Then, the active NHS esters of CA derivatives (shown in SI) reacted with the free amino groups at the periphery of polylysine in the presence of triethylamine. Telodendrimers were precipitated and washed with chilled ether. The dry polymer product was dissolved in water and purified via dialysis (MWCO: 3500 Da) against pure water.

**Preparation and Characterization of Drug-Loaded Micelles.** PTX was loaded into telodendrimer micelles via a dry-down (evaporation) method as described previously.<sup>12</sup> Briefly, 20 mg of telodendrimer along with 4 mg of paclitaxel were first dissolved in CHCl<sub>3</sub> and evaporated on rotavapor to obtain a homogeneous dry polymer film. The film was reconstituted in 1 mL phosphate-buffered solution (PBS), followed by sonication for 30 min to allow micelle dispersion. No precipitation was observed with the monodispersed particle size from 15 to 30 nm during DLS measurement, which indicated the complete drug loading. To track the biodistribution of nanoparticles, hydrophobic NIRF dye DiD was coencapsulated with PTX into the micelles using the same method as described above. The particle sizes of the micelle solution were measured via a DLS particle sizer. Finally, the micelle formulation was filtered with a 0.22  $\mu$ m filter to sterilize the sample.

The encapsulation of DOX into the polymeric micelles was carried out by following the procedure described previously. Briefly, 1 mg of DOX-HCl was stirred with 3 mol equiv of triethylamine (TEA) in chloroform (CHCl<sub>3</sub>)/methanol (MeOH) (1:1, v/v) overnight to neutralize HCl in DOX-HCl. Ten mg of PEG<sup>sk</sup>-CA<sub>8</sub> or PEG<sup>sk</sup>-(CA-

$\text{4OH})_8$  telodendrimer was added into above DOX solution in chloroform/methanol and mixed, evaporated on rotavapor to obtain a homogeneous dry polymer film, and further dried under high vacuum to further remove TEA and solvents. The film was reconstituted in 1 mL phosphate-buffered solution (PBS), followed by sonication for 30 min, allowing the sample film to disperse into micelle solution. The particle sizes of the micelle solution were measured via a DLS particle sizer. Finally, the micelle formulation was filtered with a 0.22  $\mu\text{m}$  filter to sterilize the sample.

**Hemolytic Assays.** Fresh citrated blood was obtained from healthy human volunteers. Two mL of blood was added into 10 mL of PBS, and then red blood cells (RBCs) were separated from plasma by centrifugation at 1000g for 10 min. The RBCs were washed three times with 10 mL of PBS solution, and resuspended in 20 mL PBS. Two hundred  $\mu\text{L}$  of diluted RBC suspension was mixed with polymers at serial concentrations (10, 100, 500, and 1000  $\mu\text{g/mL}$ ) by gentle vortex and incubated at 37 °C. After 0.5 h, 4 h, and overnight, the mixtures were centrifuged at 1000g for 5 min. The supernatant free of hemoglobin was measured by the absorbance at 540 nm using a UV-vis spectrometer. RBCs incubation with Triton-100 (2%) and PBS were used as the positive and negative controls, respectively. The percent hemolysis of RBCs was calculated using the following formula:

$$\begin{aligned} \text{RBC Hemolysis} = 100\% \times & (\text{OD}_{\text{sample}} - \text{OD}_{\text{PBS}}) \\ & /(\text{OD}_{\text{triton}} - \text{OD}_{\text{PBS}}) \end{aligned}$$

**Drug Release.** PTX loaded nanoformulations (500  $\mu\text{L}$ ) were placed in the dialysis bags with the MWCO of 3.5 kDa and dialyzed against 4 L of PBS at 37 °C. Five  $\mu\text{L}$  of drug solutions were sampled at the designed time intervals and PBS solution were refreshed at each measurement. The PTX concentrations were analyzed via HPLC (Simadzu LC20T) equipped with a c-18 column, and mobile phase was 55% MeCN/water. The releases of DOX from the nanoformulations were also studied using the similar dialysis method. However, the DOX concentration was monitored at 480 nm using UV-vis absorbance (Nanodrop).

**Flow Cytometric Analysis.** The quantitative cellular uptake of various DOX formulations by Raji tumor cells was analyzed by flow cytometry. Briefly,  $3 \times 10^5$  Raji cells were incubated with free DOX, DOX-PEG<sup>sk</sup>-CA<sub>8</sub>, or DOX-PEG<sup>2k</sup>-CA<sub>4</sub> at different DOX concentrations (1, 3, and 9  $\mu\text{M}$ ) for 30 min or 2 h at 37 °C, respectively. Then, the cells were washed with PBS three times and resuspended in PBS for the flow cytometry analysis using the Fortessa (Becton Dickinson, San Jose, CA). Cell-associated DOX was excited with an argon laser (488 nm), and fluorescence was detected at 560 nm; 10,000 events were collected for each sample.

**Cell Culture and MTS Assays.** Ovarian cancer cell line SKOV-3, colon cancer cell line HT-29, breast cancer cell line MDA-MB-231 and lymphoma Raji cell line were purchased from American Type Culture Collection (ATCC; Manassas, VA, U.S.A.). Ovarian cancer cell line SKOV-3, colon cancer cell line HT-29, and lymphoma Raji cell line were purchased from American Type Culture Collection (ATCC; Manassas, VA, U.S.A.). All these cells were cultured in McCoy's 5A Ovarian cancer cell line SKOV-3, colon cancer cell line HT-29, breast cancer cell line MDA-MB-231 and lymphoma Raji cell line were purchased from American Type Culture Collection (ATCC; Manassas, VA, U.S.A.). SKOV-3 and HT-29 cells were cultured in McCoy's 5A medium and MDA-MB-231 and Raji cells were cultured with RPMI 1640 medium supplemented with 10% fetal bovine serum (FBS), 100 U/mL penicillin G, and 100  $\mu\text{g/mL}$  streptomycin at 37 °C using a humidified 5% CO<sub>2</sub> incubator. SKOV-3 cells were seeded in 96-well plates at a density of 10,000 cells/well 24 h prior to the treatment. Empty micelles and various formulations of PTX with different dilutions were added to the plate and then incubated in a humidified 37 °C, 5% CO<sub>2</sub> incubator. After 72 h incubation, CellTiter 96 Aqueous Cell Proliferation Reagent, which is composed of MTS and an electron coupling reagent PMS was added to each well according to the manufacturer's instructions. The cell viability was determined by measuring the absorbance at 490 nm using a microplate reader (BioTek Synergy 2 Microplate Reader). Untreated cells served

as a control. Results are shown as the average cell viability  $[(\text{OD}_{\text{treat}} - \text{OD}_{\text{blank}})/(\text{OD}_{\text{control}} - \text{OD}_{\text{blank}}) \times 100\%]$  of triplicate wells.

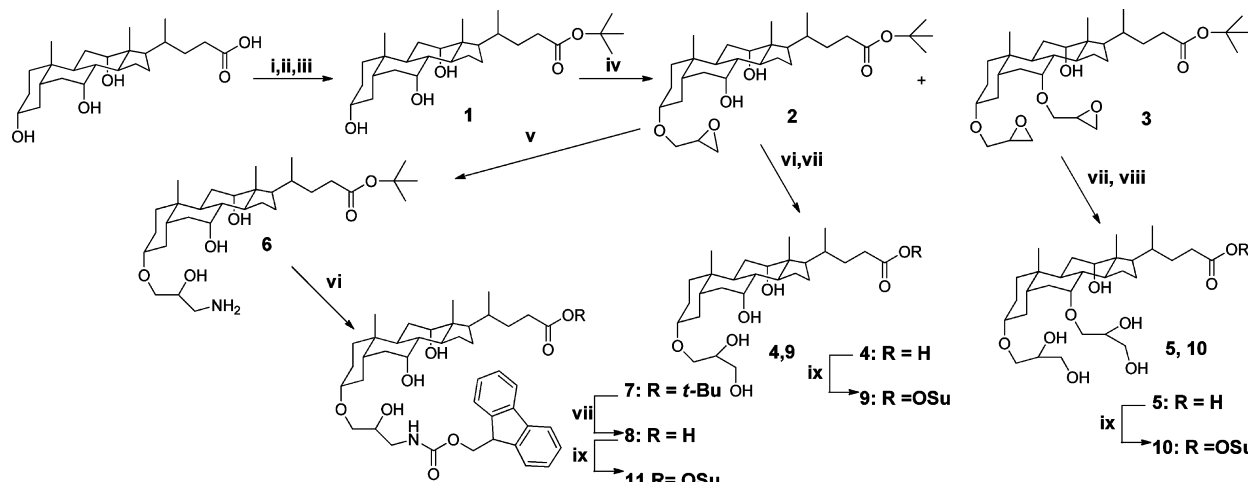
**Animal Xenograft Models and the Fluorescence Animal Imaging.** Female athymic nude mice (Nu/Nu strain), 6–8 weeks age, were purchased from Harlan. All animals were kept under pathogen-free conditions according to AAALAC (Association for Assessment and Accreditation of Laboratory Animal Care) guidelines and were allowed to acclimatize for at least 4 days prior to any experiments. All animal experiments were performed in compliance with institutional guidelines and according to protocol approved by the Committee for the Humane Use of Animals of the State University of New York Upstate Medical University. A subcutaneous colon cancer xenograft mouse model was established by injecting  $1 \times 10^7$  HT-29 or MDA-MB-231 cancer cells in a 100  $\mu\text{L}$  of mixture of PBS and Matrigel (1:1 v/v) subcutaneously at the right flank in female nude mice.

Nude mice with subcutaneous tumors of an approximate 8–10 mm in diameter were subjected to *in vivo* NIRF optical imaging. At different time points postinjection of DiD- and PTX-coloaded micelles formed by telodendrimer II (the mass ratio of DiD and PTX within nanocarrier was 0.25:1:10), mice were scanned using a IVIS-200 small animal imager at cy5.5 excitation and emission channels. The mice were anaesthetized by isoflurane gas before and during each imaging. After *in vivo* imaging, animals were euthanized by CO<sub>2</sub> overdose at 48 or 72 h after injection. Tumors and major organs were excised and imaged with the IVIS-200 small animal imager.

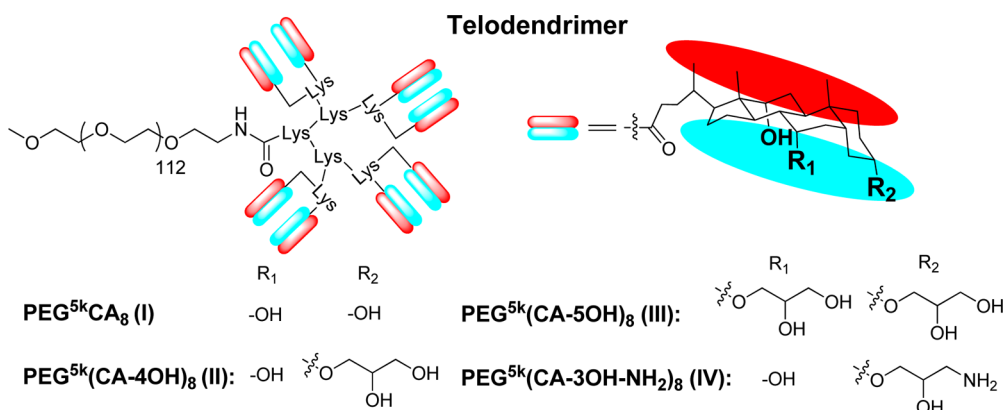
**Molecular Dynamics Simulations: Simulated Annealing.** Advanced molecular dynamics simulations were performed to identify the most stable structures of CA dimers in polar (water) and nonpolar (decane) solvents. The initial structures of CA dimers were generated in the ChemBio 3D Ultra 13.0.0.3015 software followed by molecular dynamics simulations in GROMACS molecular dynamics package 4.5.<sup>11</sup> GROMOS96 45a3 force field<sup>13</sup> was used to model CA dimers and decane, while water was modeled using the SPC/E potential.<sup>14</sup> Each of the dimers was subjected to energy minimization in vacuum using the steepest descent algorithm; however, to explore the potential energy landscape and to identify a global minimum energy geometry, simulated annealing (SA) method was employed. For each of the CA dimers, a set of 1000 independent annealing simulations were performed from randomly selected starting structures generated by a canonical NVT ensemble simulation run at  $T = 1000$  K. The annealing was then performed by gradually reducing the temperature from 1000 to 5 K over 1 ns. Each of the 1000 independent annealing profiles were analyzed to identify the one that led to the most stable structure. The minimum energy structure was then solvated in water and decane and equilibrated using isothermal-isobaric NPT ensemble at  $T = 300$  K. The production molecular dynamics runs were performed at 300 K for 100 ns to calculate the average PSA and representative equilibrium structure geometries.

## RESULTS AND DISCUSSION

**Synthesis of the Cholic Acid Derivatives.** Cholic acid, the key building block in telodendrimers, is known to have strong membrane activity as a small-molecule surfactant.<sup>9</sup> The membrane activity of the telodendrimer micelles is believed due to the facial amphiphilic structure of CA subunit, which self-assembles through hydrogen bonding with the hydrophobic surfaces exposed to the lipid bilayer. It has been reported that the oligomer of cholic acid (so-called molecular umbrella) can effectively deliver hydrophilic biomacromolecules through the phospholipid bilayer membrane.<sup>10</sup> Also, the insertion of the assembled dimers or tetramers of CA into the phospholipid's bilayer membrane have been reported to form artificial ion channels, where hydrophilic hydroxyl groups are sheltered from the hydrophobic lipids.<sup>15</sup> Therefore, the disruption of the packing between the hydrophilic surfaces of oligo-cholic acid is expected to reduce the plasma membrane lytic activity of these types of molecules and the PEG-block-oligoCA telodendrimers. In this study, glycerol and amino-glycerol have been introduced

**Scheme 1.** Synthesis of the Building Blocks for Telodendrimers<sup>a</sup>

<sup>a</sup>Reagents and conditions: (i) TFAA, anhydrous THF, 0–5 °C, 1.5 h; (ii) *t*-BuOH, below 5 °C, then at rt for 7 h; (iii) NH<sub>3</sub>·H<sub>2</sub>O (20–30%), 0–5 °C for 12 h, then rt for 4 h; (iv) epichlorohydrin, 50% NaOH, (*n*-Bu)<sub>4</sub>NH·30 H<sub>2</sub>O, CH<sub>2</sub>Cl<sub>2</sub>, rt, 16 h; (v) NH<sub>3</sub> in MeOH (7 M), LiCl (1.2 equiv) in a sealed container, rt, 24 h; (vi) Fmoc-OSu (1.2 equiv), DIEA (1.5 equiv), CH<sub>2</sub>Cl<sub>2</sub>, 12 h; (vii) 50% TFA in CH<sub>2</sub>Cl<sub>2</sub>, 0 °C, 30 min; (viii) LiOH water solution (10 equiv), rt, 18–36 h; (ix) HOSu (1.2 equiv), DCC (1.2 equiv), CH<sub>2</sub>Cl<sub>2</sub>, rt, 12 h.

**Scheme 2.** Schematic Structures and Nomenclature of Telodendrimers with CA and the Derivatives As Building Blocks

into the 3 $\alpha$ - and 7 $\alpha$ -OH or 12 $\alpha$ -OH groups of CA via ether bond formation to increase the steric hindrance while maintaining the facial amphiphilicity of CA (Scheme 1).

First, the carboxylic acid of CA was protected via an acid labile *tert*-butyl ester via an intermediate of the hybrid anhydride with trifluoroacetic acid (TFA). A white powder of CA *tert*-butyl ester 1 was obtained with a yield over 97%. Next, epichlorohydrin was conjugated onto hydroxyl groups of CA in the presence of aqueous sodium hydroxide. Through flash column, the monosubstituted 2 and diepoxy substituted compound 3 were separated with the yield of 44.7% and 14.5%, respectively. It should be mentioned that the diepoxy-substituted compound 3 may be a mixture of the compounds of 3,5-disubstituted and 3,7-disubstituted species due to the similar reactivity of 5-OH and 7-OH groups. It was evidenced via the partial decrease of the proton signals on both 5' and 7' carbons (3.82 and 3.93 ppm), which corresponds to the C–H with the unsubstituted hydroxyl groups (Figure S1 in SI). In addition, two new peaks appeared at 3.3 and 3.4 ppm, indicating the graft of glycerol onto both 5' and 7' carbons via ether groups. In this study, we did not attempt to separate these two isomers, since they may have very similar physical properties in telodendrimers. The *tert*-butyl ester of mono-

and diepoxy-substituted compounds 2 and 3 were cleaved via a treatment with 50% of TFA in DCM at 0 °C. In the next step, the epoxy groups were opened via the treatment with lithium hydroxide solution to yield diol derivatives 4 and 5 at yields of 84.4% and 36.5%, respectively. In addition, monoepoxy-derived compound 2 was treated with an NH<sub>3</sub> solution in methanol in the presence of LiCl as a catalyst to introduce amino groups on the polar surface of CA (compound 6). Furthermore, free amine in compound 6 was protected via Fmoc-OSu, then *tert*-butyl ester in compound 7 was removed via the treatment of 50% TFA in DCM to yield Fmoc-protected amino cholic acid 8 with an 88.4% yield after flash column purification. All the CA derivatives with free carboxylic acids 4, 5, and 8 were activated via coupling with HOSu using DCC as a condensation reagent to yield active esters 9, 10, and 11, respectively, for telodendrimer conjugation. All the NMR spectra (Figure S1 in SI) and mass spectra (Figure S2 in SI) indicated the correct chemical structures of these intermediates of CA derivatives.

**Preparation and Characterization of Telodendrimers.** Following our previous procedure,<sup>5</sup> we further synthesized the telodendrimers I, II, III, and IV (Scheme 2) via liquid peptide chemistry using CA and CA derivatives as building blocks to cap the periphery of dendritic polylysine. The proton NMR

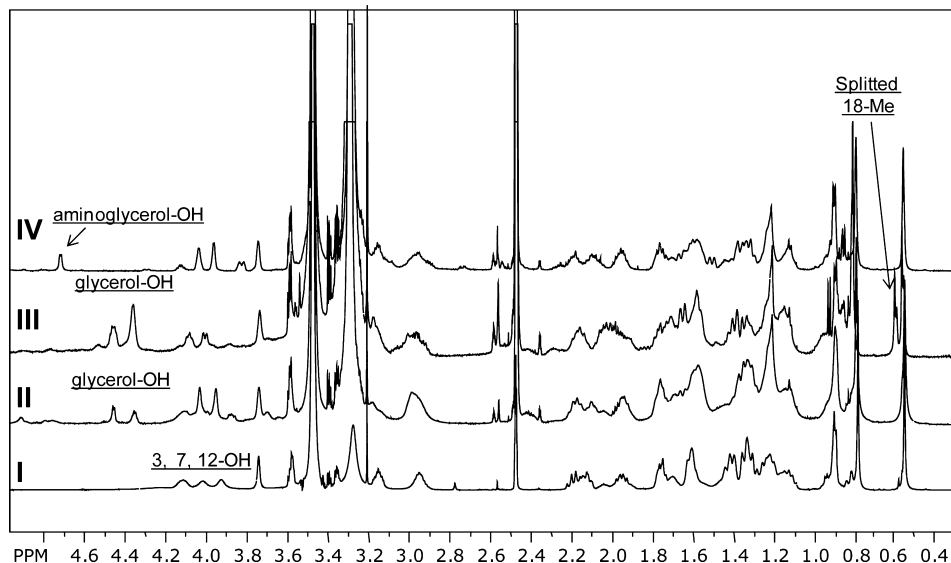


**Figure 1.** Proton NMR spectra of the telodendrimers with CA and CA derivatives as building blocks.

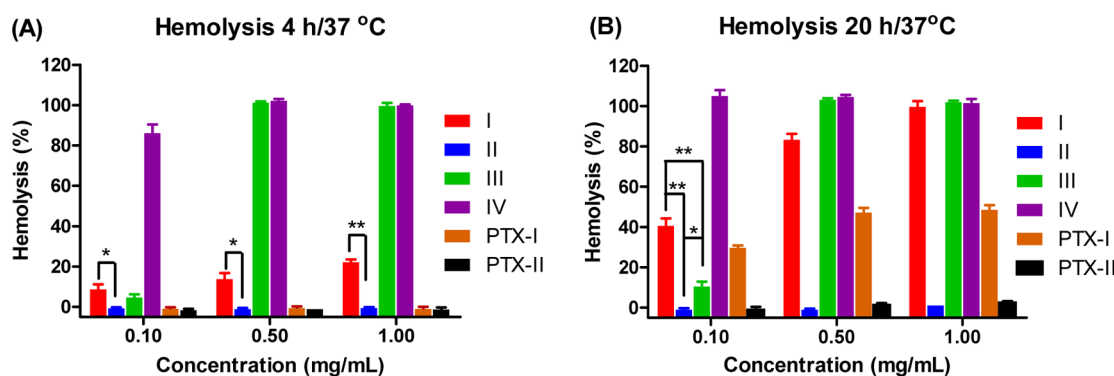


**Figure 2.** Hemolytic properties of telodendrimers with different glycerol modifications and with/without PTX loading after incubation with human red blood cells for 4 h (A) and 20 h (B). The triplicated data are presented as mean  $\pm$  SD (\*:  $p < 0.05$ ; \*\*:  $p < 0.005$ ).

spectra of these telodendrimers are shown in Figure 1. The proton signal of 3-OH on CA disappeared in telodendrimers II and IV, and new hydroxyl groups on glycerol and amino-glycerol appeared in telodendrimers II and IV, indicating the expected 3-position glycerol substitution. Five hydroxyl groups on diglycerol-substituted compound 5 were observed in the proton NMR spectrum (Figure S1 in SI), which was also shown in the NMR spectrum of telodendrimer III. The complete disappearance of the 3-hydroxyl group and the partially decreased proton signals of both 7- and 12-hydroxyl groups on CA in telodendrimer III were observed in the NMR spectrum (Figure 1). In addition, the substitution on 12-OH caused the proton signal of C-18 methyl groups shifted partially toward the low field from 0.57 to 0.60 ppm. Similar phenomena have been reported in the literature.<sup>16</sup> The above NMR results indicated that CA-SOH derivative may have two different isomers, e.g. 3,7- and 3,12-disubstitutions. The number of cholic acid and its derivatives coupled onto the telodendrimer were calculated to be 7.4–7.6 (theoretical number of 8) via the integration of PEG proton signal and 18-methyl group on cholic acid.

As expected, the engineered telodendrimer II PEG<sup>sk</sup>(CA-4OH)<sub>8</sub> micelles exhibited negligible hemolytic properties compared with typical telodendrimer I PEG<sup>sk</sup>CA<sub>8</sub> (Figure 2) after incubation with red blood cells for both 4 and 20 h at 37

°C. After being loaded with PTX, PEG<sup>sk</sup>(CA-4OH)<sub>8</sub> micelles were observed to be nonhemolytic up to 1 mg/mL after 20 h incubation. However, 100% and 50% hemolysis were caused by the original telodendrimer I PEG<sup>sk</sup>CA<sub>8</sub> before and after PTX loading, respectively, at the same 1 mg/mL concentration. Telodendrimer IV with amino-derived cholic acid as building block shows almost 100% hemolysis even at a concentration as low as 0.1 mg/mL for a 4 h incubation period (Figure 2). It is due to the positive charges on this telodendrimer IV increasing the interaction with negatively charged cell membrane. Very surprisingly, much more hydrophilic telodendrimer III with five hydroxyl groups on each cholic acid scaffold also showed significant hemolysis at high concentrations of about 0.5 to 1 mg/mL after 4 h incubation, which was even higher than the parent telodendrimer PEG<sup>sk</sup>CA<sub>8</sub> (Figure 2). It has been reported that the bulky hydrophilic block in an amphiphilic polymer may disturb the liquid crystalline packing of lipid bilayer in addition to the effect brought by the hydrophobic block alone. In particular, block copolymers having branched polyglycerol as hydrophilic blocks show a far more pronounced effect on membrane structure as compared to copolymers with linear PEO blocks.<sup>17</sup> However, it is still unclear why the plasma membrane lytic activity of telodendrimers varied with the number of glycerols introduced on CA.

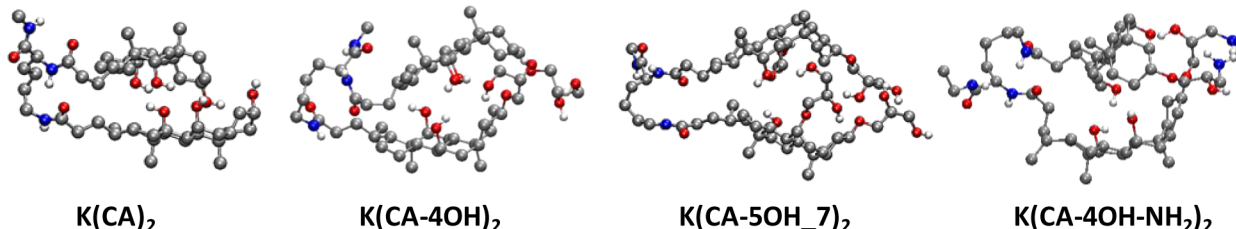


Figure 3. Energy-minimized folded conformations of the CA dimers (in vacuum) with varying glycerol substitutions displayed in two modes and orientations.

**Molecular Dynamic Simulation.** Although, it is not easy to study the interactions between micelles and plasma membrane directly via molecular simulation at the atom level, we could apply these approaches to study the conformations of the hydrophobic subunits of the telodendrimers, which directly interact with plasma membrane. It is believed that the plasma membrane lytic activity of a polymer micelle solution are caused by a small portion of the free amphiphilic polymers existing in solution rather than the intact micelles which are covered by a layer of inert hydrophilic polymer.<sup>3</sup> Polar surface area (PSA) is commonly used to characterize the permeability of a drug molecule.<sup>18,19</sup> A small molecule with a PSA less than 1.40 nm<sup>2</sup> is likely to be able to penetrate through the cell membrane.<sup>20</sup> Therefore, the PSA of the polymer subunits can be used to compare their membrane activities. The density of the polar functional groups, i.e. hydroxyl groups in cholic acid, contributes to the PSA of telodendrimers. A dimer of cholic acids bridged via a lysine, KCA<sub>2</sub>, is a subunit of telodendrimer I, which was calculated to have 3.15 nm<sup>2</sup> of PSA solely based on the functional group contribution. However, the varying conformation of a molecule may change its topological polarity significantly. Therefore, the stable conformation of the KCA<sub>2</sub> was studied via simulated annealing molecular dynamics simulations. The PSA of the most stable conformations were calculated on the basis of the topology of the molecules.

As shown in Figure 3, a hand-in-hand like hairpin conformation of KCA<sub>2</sub> with the efficient shelter of their hydroxyl groups at the interface of the complex formed via hydrogen bonding. A majority of KCA<sub>2</sub> hydrophobic surface is exposed, which favors membrane insertion and may directly contribute to the observed hemolytic properties. A considerably reduced PSA of KCA<sub>2</sub> with the minimized energy was calculated in vacuum to be 1.08 nm<sup>2</sup> (Table 1), which was much smaller than the PSA solely based on the functional group contributions (3.15 nm<sup>2</sup>). In a biological system, the interaction of polymers with the plasma membrane occurs in an aqueous condition. Therefore, a comparison of the PSA of CA dimers in the presence of water molecules may be more representative for the membrane activity of the free amphiphilic molecules in water. On the other hand, the disintegrated polymer micelle may merge with the cell membrane from the exposed hydrophobic core, especially when nanoparticles are chemically or physically anchored onto the cell membrane via targeting ligands or nonspecific interactions. In this case, the core-forming CA dimers aggregate in the hydrophobic core of the micelles. Therefore, the conformations of the CA dimers were equilibrated in hydrophobic decane to probe these scenarios. It is noticed that the molecules have small PSA after being simulated in vacuum. After equilibration with the solvent molecules (water or decane) at 300 K for 100 ns, solvent molecules could insert into the folded structures. The

**Table 1. Polar Surface Area (PSA) of the Subunit of Telodendrimers with the Minimized Energy Obtained through Simulated Annealing Molecular Dynamics<sup>a</sup>**

subunit of telodendrimers	PSA in different solvents (nm <sup>2</sup> )		
	vacuum	water	decane
K(CA) <sub>2</sub>	1.08	1.57	1.23
K(CA-4OH) <sub>2</sub>	1.19	1.65	1.34
K(CA-SOH <sub>7</sub> ) <sub>2</sub>	1.04	1.52	1.19
K(CA-SOH <sub>7/12</sub> ) <sub>2</sub>	1.09	1.47	1.21
K(CA-SOH <sub>12</sub> ) <sub>2</sub>	1.10	1.49	1.24
K(CA-3OH-NH <sub>2</sub> ) <sub>2</sub>	1.21	1.71	1.39
K(CA-3OH-NH <sub>3+</sub> ) <sub>2</sub>	1.43	2.09	1.78

<sup>a</sup>The stable structures in vacuum were first obtained by the simulated annealing process and then solvated in water or decane at 300 K and equilibrated. No annealing runs were performed in the presence of solvent. The production MD simulation runs were performed at 300 K for 100 ns to calculate the average PSA and the equilibrium structure geometries.

hydroxyl groups were exposed more, and the PSA increased, especially in aqueous conditions (Table 1). However, the dimer molecules still remained in the folded conformations restricted by the hydrogen bonding.

According to our hypothesis, we expect to see the increased PSA and the disrupted folding of the CA dimers after introducing bulky hydrophilic groups to CA. The molecular dynamics simulations revealed that the single-glycerol modified CA dimer, K(CA-4OH)<sub>2</sub>, also forms a hairpin-like folded conformation via hydrogen bonding (Figure 3). Compared to KCA<sub>2</sub> the K(CA-4OH)<sub>2</sub> dimer resulted in a lower-energy structure (Figure S3 in SI) using a simulated annealing approach that is attributed to the enhanced hydrogen bonding. However, as shown in Figure 3, the extra hydroxyl groups are exposed to the solvent molecules at the bottom of the molecular clips. As expected, the K(CA-4OH)<sub>2</sub> dimer possesses a higher PSA in vacuum (1.19 nm<sup>2</sup>) and after equilibration in water (1.65 nm<sup>2</sup>) or decane (1.34 nm<sup>2</sup>), which may prohibit the insertion of the telodendrimer into the hydrophobic lipid bilayer membrane. As shown in Figure 3, the CA dimer with diglycerol modification, possessing five hydroxyl groups on each cholic acid, K(CA-SOH<sub>7</sub>)<sub>2</sub>, forms a very stable folded conformation via an extensive hydrogen-bonding network. The stable conformations of folded K(CA-SOH<sub>7</sub>)<sub>2</sub> lead to the highest energy stabilization (Figure S3 in SI) during the annealing and folding process compared to other CA modifications. Most polar groups have been sheltered within the folded conformation, and the PSA was calculated to be the smallest at 1.04 nm<sup>2</sup> for K(CA-SOH<sub>7</sub>)<sub>2</sub> in vacuum, which is even smaller than that for KCA<sub>2</sub> in the original telodendrimer I. The possible isomers of the disubstituted CA dimers with the second glycerol on the 7' or 12' position (e.g., K(CA-

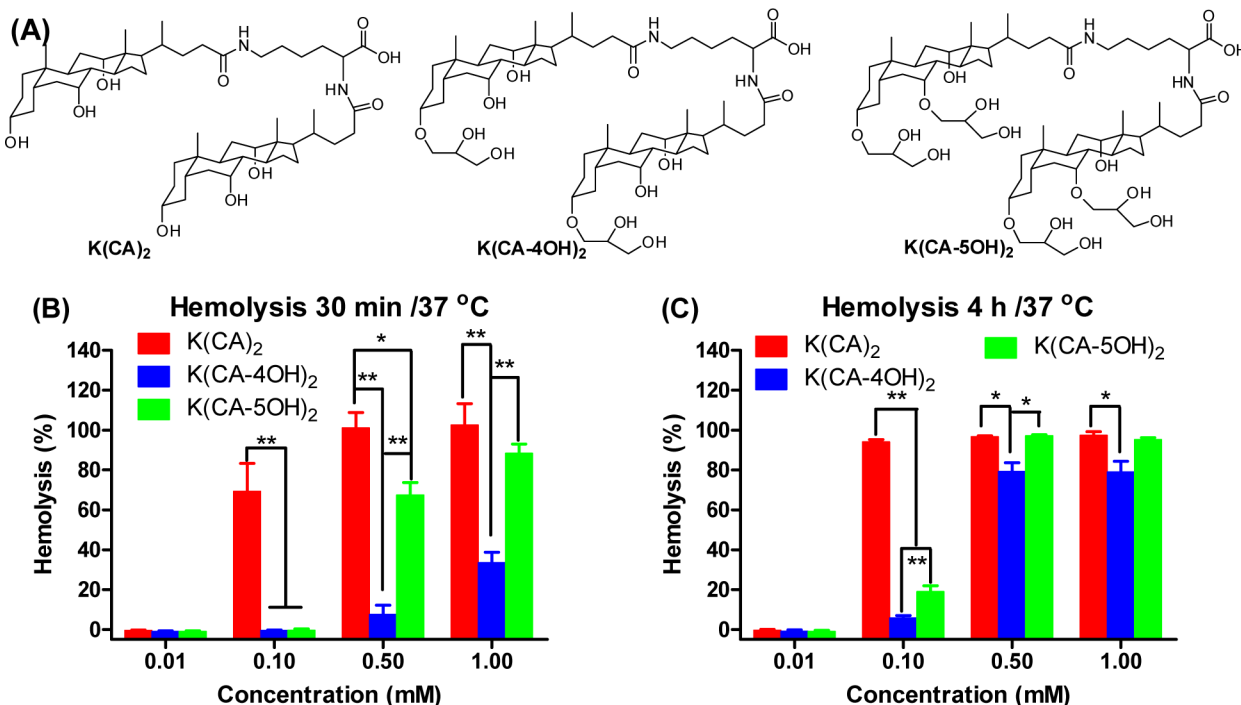


**Figure 4.** Structure of the cholic acid dimers with different glycerol substitution prepared via solution-phase organic synthesis (A); hemolytic properties of small-molecule dimers of cholic acid with different glycerol modifications after incubation with human red blood cells for 30 min (B) and 4 h (C). The triplicate data are presented as mean  $\pm$  SD (\*:  $p < 0.01$ ; \*\*:  $p < 0.001$ ).

SOH\_7)<sub>2</sub>; K(CA-SOH\_12)<sub>2</sub> and K(CA-SOH\_7/12)<sub>2</sub> (Figure S4 in SI)) have the similar small PSA values and low binding energies during the simulated annealing process (Figure S3 in SI). The smaller PSA and stable conformation both contribute to the hemolytic activity of the telodendrimer III.

As shown in Figure 3, the subunit of telodendrimer IV, K(CA-3OH-NH<sub>2</sub>)<sub>2</sub>, also formed a folded conformation via hydrogen bonding to partially shelter the polar groups after equilibration through molecular dynamics simulations. The PSA of the amino-derived CA dimer with an energy-minimized folded conformation was calculated to be higher, 1.21 nm<sup>2</sup> in vacuum, which is further increased to 1.43 nm<sup>2</sup> upon protonation. However, the positively charged amino groups are located at the bottom of the resulting CA dimers, which are believed to induce stronger electrostatic interactions with phospholipid bilayer cell membranes. Accordingly, a 100% hemolysis was observed for telodendrimer IV even at 0.1 mg/mL after a 4 h incubation (Figure 2), which is the combination of charge and hydrophobic effects.

**Synthesis of Dimers of Cholic Acid Derivatives to Validate the Theoretical Prediction.** The above molecular simulation studies have clearly revealed the potential SPR between CA modification and the hemolytic activity of telodendrimers. However, the direct validation of the computational simulation might be essential for applying these approaches to study the SPR of nanocarriers. Therefore, cholic acid dimers studied in molecular simulation were synthesized and evaluated. Cholic acid dimers with the different glycerol substitution were prepared via solution-phase peptide chemistry (Figure 4A). As shown in the SI, K(CA)<sub>2</sub>, K(CA-4OH)<sub>2</sub>, and K(CA-5OH)<sub>2</sub> have been characterized with proton NMR (Figure S5 in SI) and MALDI-TOF MS (Figure S6 in SI), demonstrating the right structures. The hemolysis properties of these three dimers were tested directly via red blood cell

incubation. It is expected that these small molecules showed higher hemolysis compared with telodendrimers, due to the lack of PEG sheltering. As predicated in the MD simulation, the K(CA-4OH)<sub>2</sub> exhibited a significantly lower membrane activity in hemolysis assays than both K(CA-SOH)<sub>2</sub> and K(CA)<sub>2</sub> for 30 min and 4 h incubation (Figure 4B,C). It was also observed that unmodified K(CA)<sub>2</sub> showed a significantly higher membrane activity than K(CA-5OH)<sub>2</sub>, especially at relatively low concentration of 0.1 mM. However, telodendrimer I PEG<sup>sk</sup>CA<sub>8</sub> showed significantly lower hemolysis than telodendrimer III PEG<sup>sk</sup>(CA-5OH)<sub>8</sub> after 4 h incubation (Figure 2A). This may due to the better integrity of PEG<sup>sk</sup>CA<sub>8</sub> micelles with the relative low CMC (as discussed below) compared with PEG<sup>sk</sup>(CA-5OH)<sub>8</sub> micelles, which are more hydrophilic with higher CMC. The dynamic nature of PEG<sup>sk</sup>(CA-5OH)<sub>8</sub> micelles makes them readily interact with the plasma membrane.

**In Vitro Drug Encapsulation and Anticancer Effects.** The above chemical modifications of CA on the hydrophilic surface maintained the facial amphiphilic property of CA within the telodendrimer, which ensured the formation of micellar nanoparticles for drug loading. However, such modification on CA increased the critical micellization concentrations (CMCs) of the telodendrimers. The CMCs were measured via the classic pyrene 1:3 method<sup>21</sup> to be 17.4  $\mu$ g/mL, 24.2  $\mu$ g/mL, 95.9  $\mu$ g/mL and 49.3  $\mu$ g/mL for telodendrimers I, II, III, and IV, respectively (Figure S-7 in SI). The significantly increased CMCs for telodendrimers III and IV indicated the higher free polymer concentration in micelle solutions, which may further contribute to the enhanced hemolytic properties. The telodendrimer II PEG<sup>sk</sup>(CA-4OH)<sub>8</sub> showed similar particle size and stability before and after PTX loading at 3/20 drug/polymer ratio, compared with the original telodendrimer I PEG<sup>sk</sup>CA<sub>8</sub>, due to the similar structures and CMCs. In

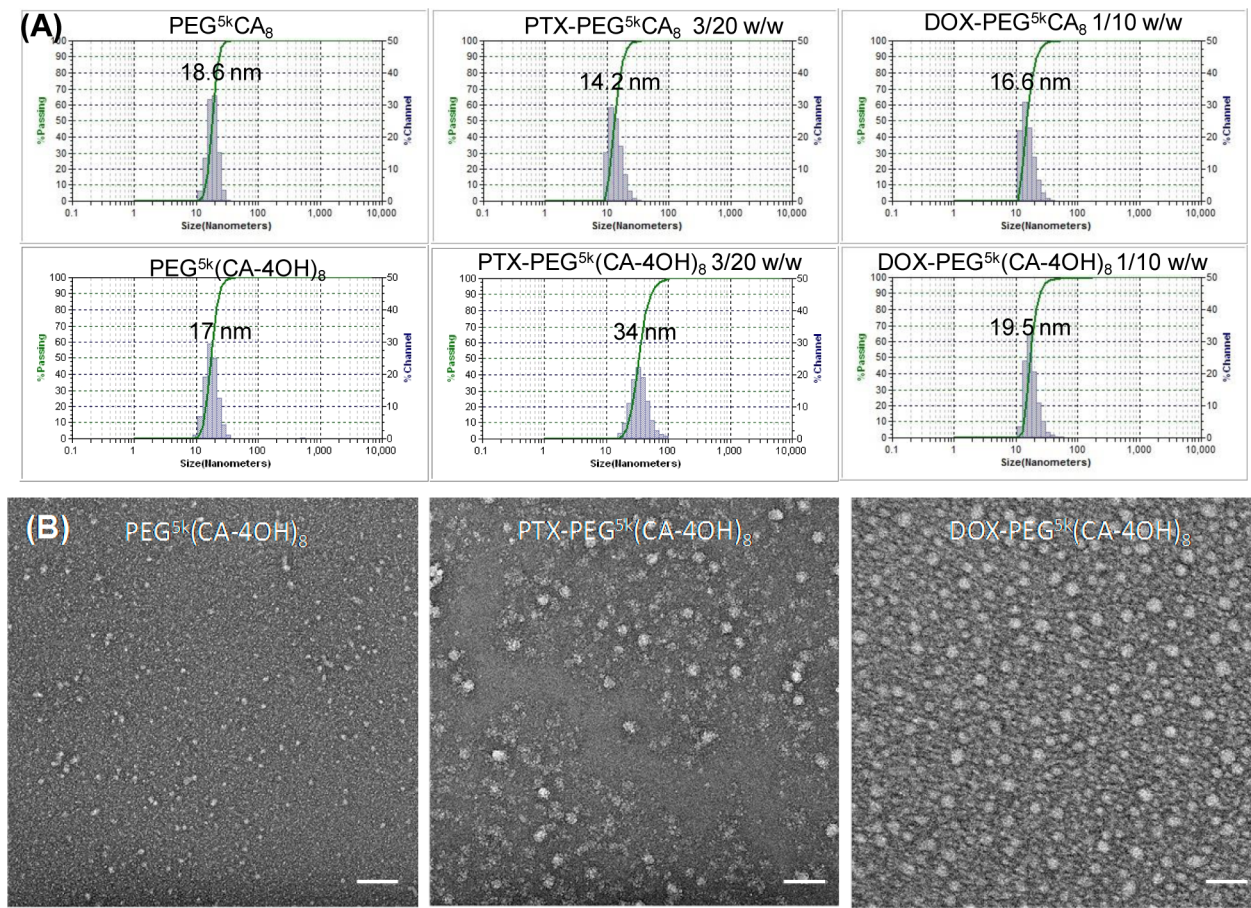


**Figure 5.** (A) DLS particle sizes of telodendrimer I and II and the micelles loaded with PTX and DOX. The mean particle sizes are presented based on area-distribution; (B) TEM images of telodendrimer II after being loaded with PTX and DOX, respectively, with uranyl acetate staining (scale bar: 100 nm).

addition, telodendrimers I and II both exhibited good loading capacity and stability for another anticancer drug, doxorubicin (DOX), at 1/10 drug/polymer w/w ratio. The particle sizes have been detected via DLS to be 34 and 19.5 nm with narrow distribution, respectively (Figure 5A). At these PTX and DOX loading ratios, clear micelle solutions were obtained without any drug precipitation observed both by eye and by DLS analysis, which indicated the complete drug loading efficiency. Further, no drug precipitation was observed from these PTX and DOX nanoformulations after storages for weeks at 4 °C. The TEM studies have revealed the spherical micelles formed by telodendrimer I before and after PTX and DOX encapsulation.<sup>6,22</sup> In this study, we also utilized TEM to study the morphology of the nanoparticles formed by  $\text{PEG}^{5k}(\text{CA}-4\text{OH})_8$ . Narrow dispersed, homogeneous spherical nanoparticles were observed (Figure 5B), which is similar to the DLS analysis (Figure 5A).

On the contrary, telodendrimer III can only assemble into smaller particles with heterogeneous distributions, e.g. 1 nm and 5 nm sizes. It is due to the overwhelming hydroxyl groups introduced to the CA polar surface, which broke the balance of the amphiphilicity of telodendrimers. After PTX loading (2:10, w/w, PTX/III), the sizes of the micelles increased to 62 nm with a small portion of larger sizes at 295 nm (Figure S8 in SI). Telodendrimer IV was observed to aggregate into micelles about 343 nm in size in pure water solution, which were reduced to about 11 nm upon adjusting pH to 5.5 due to the

increased polarity and charge repulsion of positively charged amino groups. Such PTX-loaded nanoparticles (2:10 w/w PTX/III) exhibited heterogeneous size distribution of 51 and 341 nm in PBS (Figure S9 in SI), which is not preferred for in vivo applications. As expected, telodendrimers III and IV exhibited poor DOX loading properties. The drug release of both PTX and DOX from the telodendrimer II were observed to be slightly slower than those from telodendrimer I (Figure 6A,B), which may due to the stronger hydrogen bonding. PTX released slowly from both nanocarriers with 50% drug release at about 18 h; in contrast, burst releases were observed for DOX and 50% of drug released at 8 h, due to the better water solubility of drug molecules.

Given the lowered membrane activity for telodendrimer II, one may ask whether it will decrease the cell uptake and lower the efficacy of the encapsulated chemodrugs? To address this issue, we performed the quantitative flow cytometry study to analyze the cell uptake of the chemodrugs. Doxorubicin is a fluorescent anticancer drug molecule, which was loaded in nanocarriers for cell uptake study in flow cytometry experiments. As shown in Figure 6C,D, the quantitative flow cytometric analysis demonstrated the similar cell uptake for free DOX and DOX loaded in telodendrimer micelles in Raji cells after 30 min and 2 h incubation at different drug concentrations. The cellular uptakes of all DOX formulations were in concentration- and time-dependent patterns. Furthermore, the in vitro cytotoxicity studies (Figure 6F) revealed

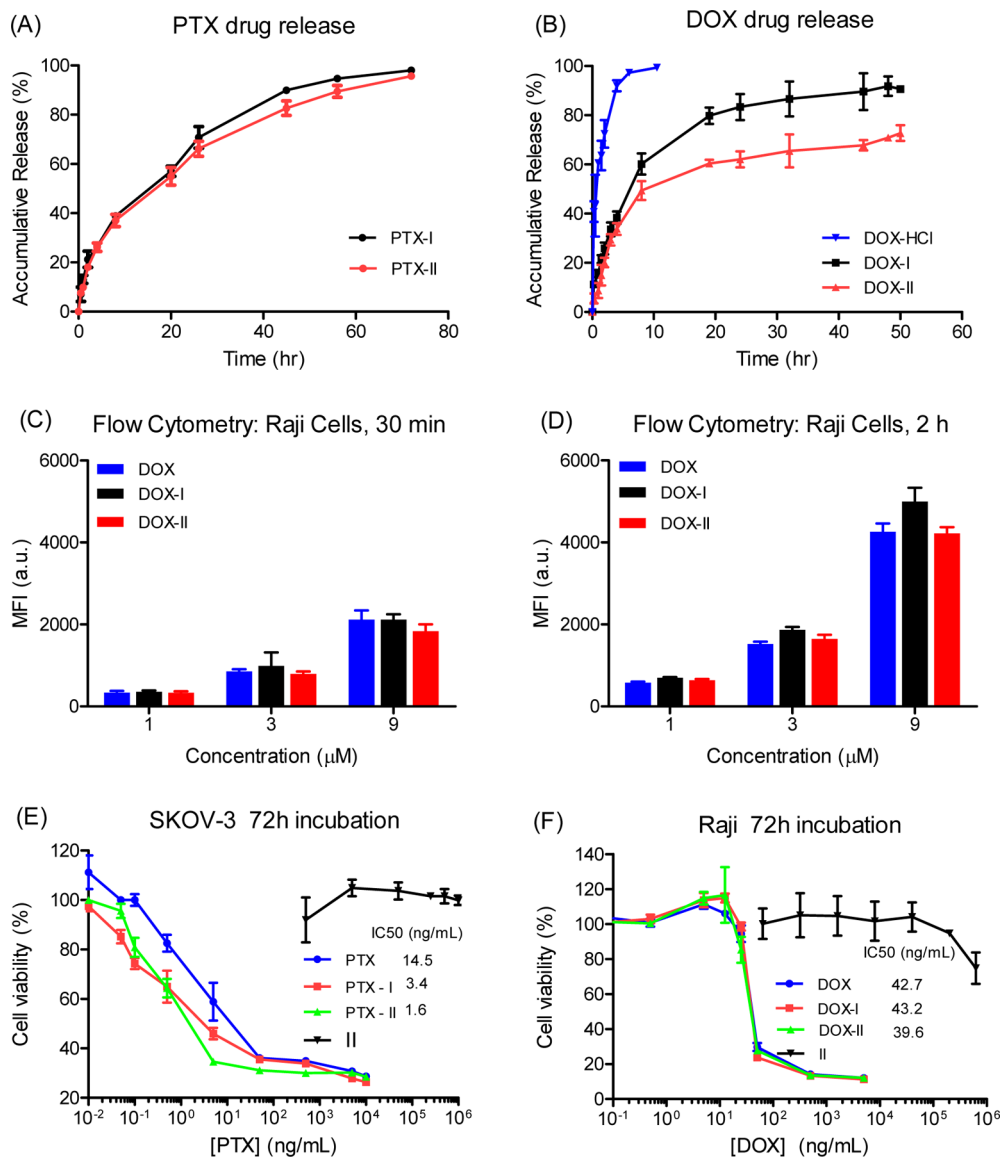


**Figure 6.** Accumulative drug release profile of PTX and DOX loaded in the nanocarrier formed with telodendrimer I (A) and monoglycerol derived telodendrimer II (B); Quantitative flow cytometry analysis of the cellular uptake of various DOX formulations by Raji cells after 30 min (C) and 2 h (D) incubation at three drug concentrations. The cell viability assays to evaluate the cytotoxicity of telodendrimer II and the anticancer effects of the micelles loaded with PTX (E) and DOX (F) on the SKOV-3 ovarian cell line and Raji lymphoma cell line, respectively.

the similar anticancer effects on the Raji lymphoma cells for the free DOX and DOX loaded in the nanocarriers I and II after 72 h incubation. Additionally the PTX-loaded telodendrimer II (IC<sub>50</sub>: 1.6 ng/mL) and PTX-loaded telodendrimer I (IC<sub>50</sub>: 3.4 ng/mL) exhibited slightly higher anticancer effects than free PTX (IC<sub>50</sub>: 14.5 ng/mL) formulated in a mixture of Cremophore EL and ethanol (1:1 v/v) in an ovarian cancer cell line, SKOV-3 (Figure 6E). This may be due to the partial precipitation of PTX from the cremophore formulation after dilution with cell culture medium. Overall, the telodendrimer II was nontoxic up to 0.5 mg/mL concentration for both cell lines.

**In Vivo Tumor-Targeted Drug Delivery.** As reported in our previous studies, telodendrimer I nanocarrier was able to target various solid tumors efficiently in animal models.<sup>5</sup> Therefore, we would like to further evaluate the biodistribution and tumor targeting properties of the optimized telodendrimers in solid tumor xenograft models, such as colon and breast

cancers after intravenous injection of telodendrimer II micelles coloaded with NIRF dye DiD and PTX. DiD is a hydrophobic near-infrared fluorescence cyanine dye, which could be stably entrapped within nanocarrier with very slow release profile (Figure S-10 in SI) and could be used as a surrogate to probe the distribution of the nanocarriers. As shown in Figure 7, the ex vivo images revealed the highest uptake of fluorescent signal in tumors compared to other organs in both tumor types. The same targeting effects for telodendrimer I were also observed previously in animal models bearing solid tumors.<sup>6</sup> The free DiD administration led to a relatively low accumulation in tumors and significant high deposition in lung, liver, and spleen, which were significantly reduced in animals treated with the nanoformulations. As shown in Figure 7B and Figure 6D, nanocarriers might be able to deliver much higher concentrations of hydrophobic drug molecules to tumor sites (2–4 fold), compared with the free DiD injections. With the enhanced in vivo anticancer effects for the PTX formulated

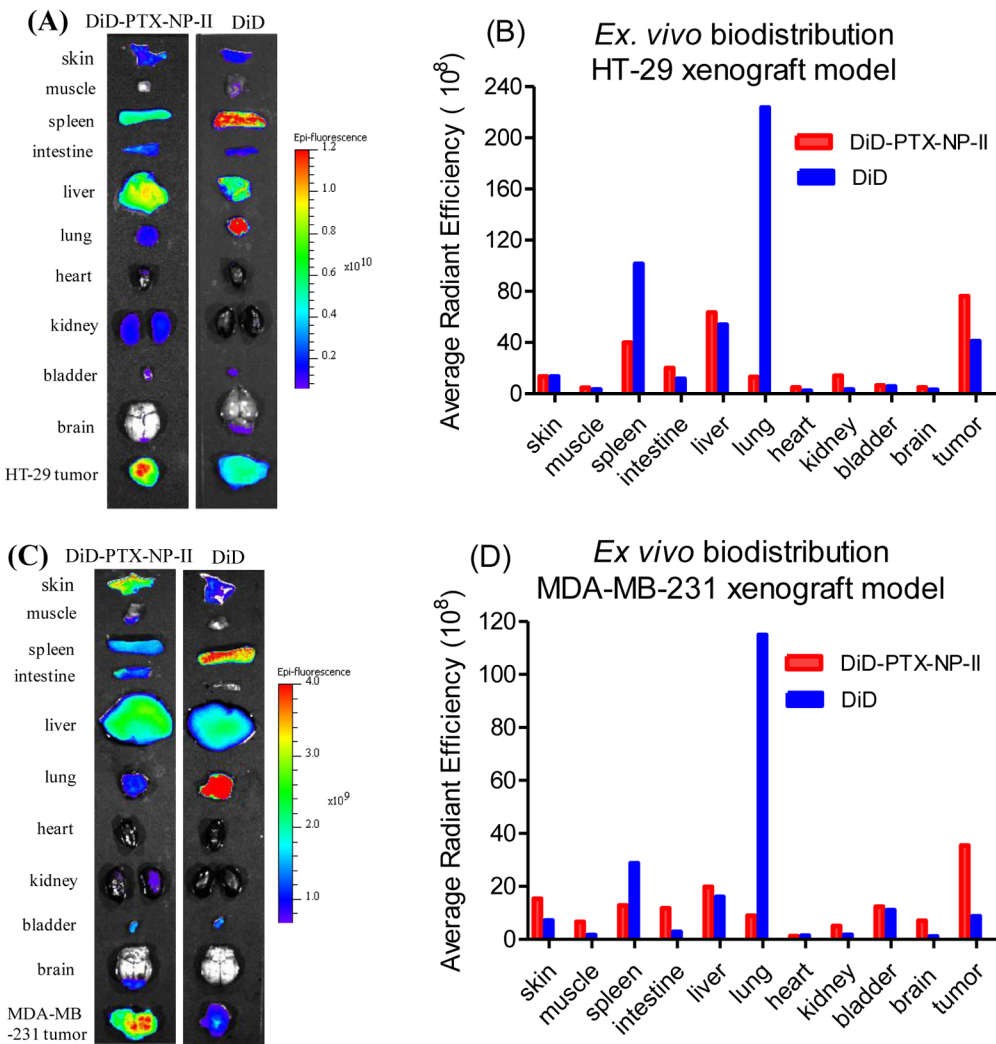


**Figure 7.** Ex vivo biodistribution of telodendrimer nanocarrier II loaded with PTX and NIRF dye DiD in colon cancer-bearing nude mice after 48 h postinjection via tail vein (A); the comparison of the average fluorescence intensity in various organs and HT-29 tumors between the animals given DiD-PTX-NP II or free dye DiD (B); ex vivo biodistribution of telodendrimer nanocarrier II loaded with PTX and NIRF dye DiD in breast cancer bearing nude mice after 72 h postinjection via tail vein (C); quantitative analysis of the average fluorescence intensity in various organs and MDA-MB-231 tumors between the animals given DiD-PTX-NP II or free dye DiD (D).

in telodendrimer I nanocarriers,<sup>6</sup> we anticipate these non-hemolytic nanotherapeutics formed by telodendrimer II will further improve the anticancer effects via efficient tumor-targeted drug delivery. The further PK/PD studies and the in vivo efficacy of this optimized nanocarrier in delivering different chemotherapeutics in animal models will be tested and reported in a separate account.

## CONCLUSIONS

The SPR of a telodendrimer system in interacting with plasma membranes has been clearly revealed via computational and experimental approaches. To minimize the hemolytic properties of telodendrimer nanocarriers, we took a rational approach to modify telodendrimer structures by introducing hydrophilic glycerol or amino-glycerol groups onto the polar surface of cholic acid. With the aid of molecular dynamics simulations, we had a better understanding of the relationship between plasma membrane lytic activity and the structural conformations of the amphiphiles. The introduction of hydrophilic monoglycerol onto the polar surface of cholic acid was predicated via molecular dynamics to be optimal in disrupting the molecular

folding of the subunit of telodendrimer and increasing the polar surface area of the complex. This was correlated with the minimal hemolytic properties observed in experiments. On the contrary, introduction of two glycerols or an amino-glycerol on each cholic acid led to the increased hemolytic properties of the resulting telodendrimers, which were correlated with the decreased PSA and the exposed positive charges in the molecular dynamics simulations, respectively. Further, the computation results have been verified in the experiments via the synthesis of the telodendrimer subunits, which were tested to be consistent with the theoretical prediction for the membrane activities. Such spatial modification of CA via monoglycerol grafting sustained the balance of the facial amphiphilicity of CA, therefore maintaining the PTX and DOX loading capacity, stability, and anticancer effects of the nanotherapeutics. Given the nonhemolytic property, efficient cancer cell uptake, and the excellent in vivo tumor-targeted properties, the monoglycerol derivatized telodendrimer II has been demonstrated as a promising nanocarrier for efficient anticancer drug delivery.

## ■ ASSOCIATED CONTENT

### Supporting Information

Synthetic procedures, NMR and mass spectra, fluorescent CMC measurement, and the DLS particle sizes. This material is available free of charge via the Internet at <http://pubs.acs.org>.

## ■ AUTHOR INFORMATION

### Corresponding Author

\*E-mail: luoj@upstate.edu. Fax: 1-315-464-5143.

### Author Contributions

<sup>1</sup>C.S. and D.Y. have contributed equally to this study.

### Notes

The authors declare no competing financial interest.

## ■ ACKNOWLEDGMENTS

We greatly acknowledge Prof. Stephan Wilkens for assistance in TEM analysis. We are grateful for the financial supports from NIH/NCI R01CA140449 (Luo), Carol M. Baldwin Breast Cancer Research Foundation (Luo), and the institutional startup funds at SUNY Upstate Medical University (Luo) and at Syracuse University (Nangia).

## ■ REFERENCES

- (1) Dobrovolskaia, M. A.; Clogston, J. D.; Neun, B. W.; Hall, J. B.; Patri, A. K.; McNeil, S. E. Method for analysis of nanoparticle hemolytic properties in vitro. *Nano Lett.* **2008**, *8* (8), 2180–2187.
- (2) Jiang, Z.; Vasil, A. I.; Hale, J. D.; Hancock, R. E.; Vasil, M. L.; Hodges, R. S. Effects of net charge and the number of positively charged residues on the biological activity of amphipathic alpha-helical cationic antimicrobial peptides. *Biopolymers* **2008**, *90* (3), 369–383.
- (3) Oda, Y.; Kanaoka, S.; Sato, T.; Aoshima, S.; Kuroda, K. Block versus random amphiphilic copolymers as antibacterial agents. *Biomacromolecules* **2011**, *12* (10), 3581–3591.
- (4) Gaucher, G.; Dufresne, M. H.; Sant, V. P.; Kang, N.; Maysinger, D.; Leroux, J. C. Block copolymer micelles: Preparation, characterization and application in drug delivery. *J. Controlled Release* **2005**, *109* (1–3), 169–188.
- (5) Luo, J.; Xiao, K.; Li, Y.; Lee, J. S.; Shi, L.; Tan, Y. H.; Xing, L.; Holland Cheng, R.; Liu, G. Y.; Lam, K. S. Well-defined, size-tunable, multifunctional micelles for efficient paclitaxel delivery for cancer treatment. *Bioconjugate Chem.* **2010**, *21* (7), 1216–1224.
- (6) Xiao, K.; Luo, J.; Fowler, W. L.; Li, Y.; Lee, J. S.; Xing, L.; Cheng, R. H.; Wang, L.; Lam, K. S. A self-assembling nanoparticle for paclitaxel delivery in ovarian cancer. *Biomaterials* **2009**, *30* (30), 6006–6016.
- (7) Shao, Y.; Huang, W.; Shi, C.; Atkinson, S. T.; Luo, J. Reversibly crosslinked nanocarriers for on-demand drug delivery in cancer treatment. *Ther. Delivery* **2012**, *3* (12), 1409–1427.
- (8) Li, Y.; Xiao, W.; Xiao, K.; Berti, L.; Luo, J.; Tseng, H. P.; Fung, G.; Lam, K. S. Well-defined, reversible boronate crosslinked nanocarriers for targeted drug delivery in response to acidic pH values and cis-diols. *Angew. Chem., Int. Ed.* **2012**, *51* (12), 2864–2869.
- (9) Ilani, A.; Granoth, R. The pH dependence of the hemolytic potency of bile salts. *Biochim. Biophys. Acta* **1990**, *1027* (2), 199–204.
- (10) Janout, V.; Zhang, L. H.; Staina, I. V.; Di Giorgio, C.; Regen, S. L. Molecular umbrella-assisted transport of glutathione across a phospholipid membrane. *J. Am. Chem. Soc.* **2001**, *123* (23), 5401–5406.
- (11) Pronk, S.; Páll, S.; Schulz, R.; Larsson, P.; Bjelkmar, P.; Apostolov, R.; Shirts, M. R.; Smith, J. C.; Kasson, P. M.; van der Spoel, D.; Hess, B.; Lindahl, E. GROMACS 4.5: A high-throughput and highly parallel open source molecular simulation toolkit. *Bioinformatics* **2013**, *29* (7), 845–854.
- (12) Liu, J.; Lee, H.; Allen, C. Formulation of drugs in block copolymer micelles: Drug loading and release. *Curr. Pharm. Des.* **2006**, *12* (36), 4685–4701.
- (13) Schuler, L. D.; Daura, X.; van Gunsteren, W. F. An improved GROMOS96 force field for aliphatic hydrocarbons in the condensed phase. *J. Comput. Chem.* **2001**, *22* (11), 1205–1218.
- (14) Berendsen, H. J. C.; Grigera, J. R.; Straatsma, T. P. The missing term in effective pair potentials. *J. Phys. Chem.* **1987**, *91* (24), 6269–6271.
- (15) Kobuke, Y.; Nagatani, T. Transmembrane ion channels constructed of cholic acid derivatives. *J. Org. Chem.* **2001**, *66* (15), 5094–5101.
- (16) Singh, M.; Singh, A.; Kundu, S.; Bansal, S.; Bajaj, A. Deciphering the role of charge, hydration, and hydrophobicity for cytotoxic activities and membrane interactions of bile acid based facial amphiphiles. *Biochim. Biophys. Acta* **2013**, *1828* (8), 1926–1937.
- (17) Demina, T.; Grozdova, I.; Krylova, O.; Zhirnov, A.; Istratov, V.; Frey, H.; Kautz, H.; Melik-Nubarov, N. Relationship between the structure of amphiphilic copolymers and their ability to disturb lipid bilayers. *Biochem.* **2005**, *44* (10), 4042–4054.
- (18) Ertl, P.; Rohde, B.; Selzer, P. Fast calculation of molecular polar surface area as a sum of fragment-based contributions and its application to the prediction of drug transport properties. *J. Med. Chem.* **2000**, *43* (20), 3714–3717.
- (19) Kelder, J.; Grootenhuis, P. D. J.; Bayada, D. M.; Delbressine, L. P. C.; Ploemen, J. P. Polar molecular surface as a dominating determinant for oral absorption and brain penetration of drugs. *Pharm. Res.* **1999**, *16* (10), 1514–1519.
- (20) Palm, K.; Stenberg, P.; Luthman, K.; Artursson, P. Polar molecular surface properties predict the intestinal absorption of drugs in humans. *Pharm. Res.* **1997**, *14* (5), 568–571.
- (21) Aguiar, J.; Carpena, P.; Molina-Bolívar, J. A.; Carnero Ruiz, C. On the determination of the critical micelle concentration by the pyrene 1:3 ratio method. *J. Colloid Interface Sci.* **2003**, *258* (1), 116–122.
- (22) Xiao, K.; Luo, J.; Li, Y.; Lee, J. S.; Fung, G.; Lam, K. S. PEG-oligocholic acid telodendrimer micelles for the targeted delivery of doxorubicin to B-cell lymphoma. *J. Controlled Release* **2011**, *155* (2), 272–281.